



Role of cortical cell type and morphology in subthreshold and suprathreshold uniform electric field stimulation *in vitro*

Thomas Radman, PhD^a, Raddy L. Ramos, PhD^{b,c}, Joshua C. Brumberg, PhD^c,
Marom Bikson, PhD^a

^aDepartment of Biomedical Engineering, City College of the City University of New York, New York, New York

^bDepartment of Neuroscience, New York College of Osteopathic Medicine NYIT, Old Westbury, New York

^cDepartment of Psychology, Queens College, CUNY, Flushing, New York

Background

The neocortex is the most common target of subdural electrotherapy and noninvasive brain stimulation modalities, including transcranial magnetic stimulation (TMS) and transcranial current stimulation (TCS). Specific neuronal elements targeted by cortical stimulation are considered to underlie therapeutic effects, but the exact cell type(s) affected by these methods remains poorly understood.

Objective

We determined whether neuronal morphology or cell type predicted responses to subthreshold and suprathreshold uniform electric fields.

Methods

We characterized the effects of subthreshold and suprathreshold electrical stimulation on identified cortical neurons *in vitro*. Uniform electric fields were applied to rat motor cortex brain slices, while recording from interneurons and pyramidal cells across cortical layers, using a whole cell patch clamp. Neuron morphology was reconstructed after intracellular dialysis of biocytin. Based solely on volume weighted morphology, we developed a parsimonious model of neuronal soma polarization by subthreshold electric fields.

Results

We found that neuronal morphology correlated with somatic subthreshold polarization. Based on neuronal morphology, we predict layer V pyramidal neuronal soma to be individually the most sensitive to polarization by optimally oriented subthreshold fields. Suprathreshold electric field action potential threshold was shown to reflect both direct cell polarization and synaptic (network) activation. Layer V/VI neuron absolute electric field action potential thresholds were lower than layer II/III pyramidal neurons and interneurons. Compared with somatic current injection, electric fields promoted burst firing and modulated action potential firing times.

This work was supported in part by the NIH NS058758 to J.C.B., NS054783 01A1 S06GMOO8168 to MB, the Andy Grove Foundation, and PSC CUNY. Correspondence: Marom Bikson, PhD, 140th St and Convent Ave, CCNY BME, Steinman Hall Room T 463, New York, NY 10031.

E mail address: bikson@ccny.cuny.edu

Submitted November 11, 2008; revised March 21, 2009. Accepted for publication March 27, 2009.

Conclusions

We present experimental data indicating that cortical neuron morphology relative to electric fields and cortical cell type are factors in determining sensitivity to sub- and supra threshold brain stimulation. © 2009 Elsevier Inc. All rights reserved.

Keywords transcranial magnetic stimulation; direct current stimulation; cortex; layer; rTMS; motor threshold; functional electrical stimulation; TDCs; electroconvulsive therapy

Clinical application of transcranial magnetic stimulation (TMS) and transcranial current stimulation (TCS, encompassing transcranial direct current stimulation [tDCS], cranial electrotherapy stimulation, transcranial electric stimulation [TES], and electroconvulsive therapy) are promising noninvasive approaches for the treatment of a number of psychiatric, neurologic, and pain disorders¹⁻⁶ as well as the study of human cognitive function and neural plasticity.⁷⁻¹⁰ Because the electric field (voltage gradient) in the extracellular space induced in the brain by TMS/TCS decays with distance from the stimulating coil or electrode, the neocortex is the most common target of noninvasive electrotherapy.¹¹⁻¹⁵ Invasive cortical stimulation that uses subdural strips/arrays is indicated for a range of therapeutic and diagnostic applications, including pain and preoperative brain mapping.^{16,17}

Fundamental questions remain regarding the cellular targets of each cortical stimulation paradigm, including the relative activation of morphologically and functionally diverse groups of inhibitory interneurons and excitatory pyramidal cells.¹⁸ Stimulation waveform, direction, and frequency is thought to preferentially affect specific cortical cell types¹⁸⁻²⁰ and/or specific segments of a neuron such as axonal bends and terminations.^{11,21,22} Neuronal segments oriented toward the stimulating anode (virtual anode for electric fields induced by TMS²²) have been shown to hyperpolarize, and concomitantly the segments oriented toward the (virtual) cathode depolarize (Supplementary Figure 1).^{23,24}

The effects of electric field-induced polarization has traditionally been categorized as “subthreshold” changes in ongoing neuronal processing/timing,²⁵⁻²⁷ or “suprathreshold” stimulation that directly triggers action potentials.^{26,28,29} Clinical brain stimulation modalities, and associated therapeutic outcomes, may depend specifically on subthreshold (eg, tDCS) and/or suprathreshold (eg, TMS) neuronal effects (reviewed in Wagner et al.³⁰). Cortical cell types,³¹ distinguished by their laminar position, network connectivity, and neuronal morphology/biophysics, play-defined roles in network processing and thus merit investigation in the context of both subthreshold and suprathreshold stimulation paradigms.¹⁸

In response to the unique electric fields induced by each brain stimulation modality,^{22,32-34} neuronal membranes are considered to polarize in a “compartment” specific manner; the polarized compartments interact according to the electrotonic decay along the neuron (Supplementary Figure 1). Neuronal modeling³⁵⁻³⁸ and *in vitro*^{25,39} studies of electric

field stimulation have identified morphologic features that govern the polarization of (interacting) neuronal compartments, including branching patterns and membrane space constants. Changes of compartment angle relative to an applied electric field (eg, activating function, the second derivative of the extracellular voltage along the neuronal membrane), branch terminations, or changes in intercompartment impedance can determine the locations of entry and exit of induced transmembrane currents that lead to polarization.^{21,23,35,38,40} The neuronal space constants (λ), and related diameter of axons and dendrites, govern the axial distribution of these induced transmembrane polarizations, and therefore regulate the degree to which neuronal compartments interact.^{38,39,41,42} Concurrent polarization of individual segments of a neuronal tree can lead to complex changes in overall neuronal function by modulating cellular biophysics,^{43,44} including nonlinear voltage-gated conductances, synaptic efficacy, and action potential (AP) threshold or timing.^{23,28,29,45,46}

The goal of this study was to determine whether the distinct morphologic features of cortical cell types affect their response to stimulation by electric field. We performed whole-cell recordings, of pyramidal cells and interneurons in rat motor cortex brain slices, during uniform electric field stimulation *in vitro*. Morphologic reconstructions of biocytin-filled neurons were correlated with electrophysiologic responses to electric fields. We considered differences between cortical cell types in their response to both subthreshold and suprathreshold stimulation. These data were used to consider the cellular targets of clinical cranial stimulation therapies.

Methods

Brain slice preparation

Coronal slices (300 μ m) of primary motor cortex (M1) were prepared from male P21-25 Sprague-Dawley rats on a vibratome (Integraslice 7550 PSDS, Campden Instruments, Lafayette, Indiana) as previously described.^{25,47-49} In brief, rats were anesthetized with intraperitoneal ketamine (7.4 mg/kg) and xylazine (0.7 mg/kg) and euthanized by decapitation. After decapitation, the brain was quickly removed, blocked, and placed into ice-cold (4°C) oxygenated artificial cerebral spinal fluid (ACSF). ACSF contained (in millimolars) 125 NaCl, 26 NaHCO₃, 3 KCl,

1.6 CaCl₂, 1.5 MgSO₄, 1.25 NaH₂PO₄, and 10 glucose, aerated with 95% O₂-5% CO₂ to a final pH of 7.4. The slices were stored in a holding chamber submerged in ACSF and bubbled with a mixture of 95% O₂-5% CO₂ at room temperature. After more than 60 minutes, slices were transferred to a submerged patch-clamp recording chamber maintained at 36°C.

In some experiments, the glutamatergic transmission blockers CNQX (AMPA receptor antagonist, 20 μ M) and APV (NMDA receptor antagonist, 50 μ M) were added to the perfusate (Sigma-Aldrich, St. Louis, Missouri).

Whole-cell patch clamp recording and data acquisition

Conventional whole-cell patch clamp recording techniques were used to measure activity from neurons in M1. Neurons were visualized with IR-DIC illumination (Olympus BS51WI, Center Valley, Pennsylvania), and identified according to layer and gross morphology. Patch pipettes (approximately 4-7 M Ω tip resistance) were pulled on a Flaming/Brown microelectrode puller (P-97, Sutter Instruments, Novato, California). Pipettes were filled with (in millimolars) 120 KGlu, 10 NaCl, 20 KCl, 10 HEPES, 2 Mg-ATP, 0.3 Na-GTP, 0.5 EGTA, and 0.3-1% biocytin (wt/vol) for subsequent visualization of the neurons. Electrophysiologic signals were amplified (Axoclamp-2B, Molecular Devices, Sunnyvale, California) and filtered at 10 kHz (FLA01, Cygnus Technologies, Delaware Water Gap, Pennsylvania), then digitized (Power 1401 ADC/DAC, Cambridge Electronic Design, Cambridge, United Kingdom). Offline analysis of action potential and passive membrane properties were performed using Signal 3 (Cambridge Electronic Design). On obtaining a high-resistance seal (>1 G Ω) with a neuron but before establishing whole-cell configuration, the microscope objective (water immersion; 40 \times , Olympus) was removed from the bath to reduce perfusate level (and related electric field) nonuniformities. Once a stable whole-cell configuration was obtained (resting membrane potential of less than -55 mV, overshooting action potentials, generation of repetitive APs in response to a depolarizing current pulse), neurons were classified according to discharge pattern in response to a constant depolarizing current pulse (100 milliseconds) as intrinsically bursting, fast spiking or regular spiking.^{47,50,51}

Generation of uniform electric fields and quantification of neuronal response

Uniform electric fields were generated across individual slices by passing current between two parallel Ag/AgCl electrodes^{25,48,52-56} placed on the bottom of a customized submerged chamber; the wires were parallel to the direction of perfusate flow and measuring 15-16 mm long and 7-9 mm apart. Field waveforms were generated by

a Power 1401 ADC/DAC (Cambridge Electronic Design) and converted to a controlled current source by up to three parallel stimulus isolation units (2200, 2300, A-M Systems, Carlsborg, Washington). Because of the reduced current density caused by the deeper fluid levels in submerged patch recording chambers, to achieve electric field magnitudes the same as those applied in previous studies that used interface recording chambers,^{25,48} an order of magnitude greater current intensity was necessary. This, in turn, limited the maximum electric field applied (for example, in determining AP thresholds). The electric field (mV/mm) in the chamber was measured by two recording electrodes separated by 1 mm and calibrated to the current passed through the Ag/AgCl electrodes. The convention of electric field polarity used in the current report refers to the anode on the pial side of the cortex.

The voltage recorded by a field electrode (placed within 50 μ m of the recorded neuron) was subtracted from the intracellular potential to obtain the transmembrane voltage and used to compensate for the exogenous electrical artifact. Post hoc corrections for voltage differences between the field and intracellular electrode (measured at the termination of each recording) were made by scaling the electric field command waveform to the interelectrode difference and subtracting from the recorded transmembrane voltage. We note that this creates a residual onset and offset artifact that was not included in our analysis. For each cell, the somatic steady-state transmembrane voltage response to approximately 5 mV/mm electric field steps (Figure 1, B), up to approximately ± 30 mV/mm, were linearly fit, the slope of which determined the cell-specific subthreshold somatic polarization per unit electric field applied (Figure 2), in units of millivolts of polarization per millivolt/millimeter of electric field (mV*(mV/mm)⁻¹). This slope, which has also been referred to as "mV per mV/mm," "coupling coefficient," and "cell susceptibility,"^{25,48,52} reduces to millimeters and shall be referred to here as polarization length, λ_p .

Suprathreshold electric fields induced nonlinear polarizations with characteristic excitatory postsynaptic potential (EPSP) waveforms⁴⁹ and/or APs, as determined by visual inspection. Averages are reported as mean \pm standard error. Statistics within a 95% confidence interval have been labeled as significant.

Morphologic reconstruction of biocytin-filled neurons

After recordings, slices were placed in cold fixative (4% paraformaldehyde in 0.1 M phosphate buffer) and kept at 4°C for no more than 2 weeks. Biotin-avidin-horseradish peroxidase (HRP) histochemistry was performed as previously described.⁵⁷⁻⁵⁹ Briefly, sections were first placed in 1% H₂O₂/0.5% MEOH and phosphate buffer saline (PBS)

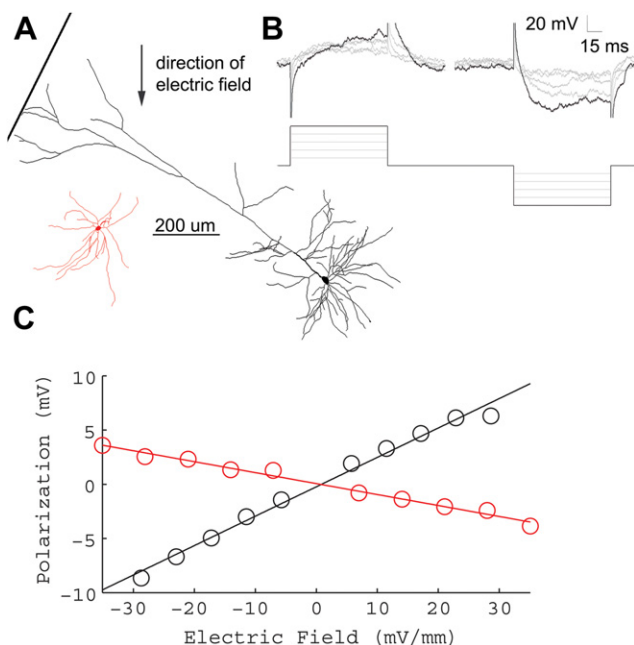


Figure 1 Subthreshold electric fields polarize cortical neuronal soma linearly. **A**, Example morphologic reconstruction of a LV pyramidal neuron (black), and LV fast spiking interneuron (red). **B**, Incrementing electric field steps of 5.8 mV/mm (bottom) linearly polarize cell soma (top). Traces shown are from LV regular spiking pyramidal neuron of **A** (top). **C**, Summary of the polarization per electric field for the neurons shown in **A**. The slope of the fitted line determines the subthreshold field polarization sensitivity for each neuron. LV pyramidal neuron (black) = $0.27 \text{ mV} \cdot (\text{mV/mm})^{-1}$, LV fast spiking interneuron (red) = $0.02 \text{ mV} \cdot (\text{mV/mm})^{-1}$.

to quench endogenous peroxidase activity. After three washes in PBS, sections were permeabilized for 1 hour in PBS containing 0.2% Triton-X (Sigma-Aldrich). Sections were then placed in an avidin-HRP mixture (ABC Kit, Vector Labs, Burlingame, California) for 2 hours. After three washes in PBS, sections were reacted in 0.05% diaminobenzidine/0.015% H_2O_2 . Slices were washed in PBS, mounted onto gelatin-coated slides, and coverslipped in DPX (Electron Microscopy Sciences, Hatfield, Pennsylvania). For three-dimensional morphologic reconstructions, the NeuroLucida system (MicroBrightfield, Williston, Vermont) was used in conjunction with an Olympus BX51 microscope using 4 \times (0.1 numerical aperture [NA]), 10 \times (0.4 NA), and 60 \times (1.4 NA, oil) objectives. Digital images were taken using an Optronics Microfire camera (Optronics Inc, Muskogee, Oklahoma). Morphologic measurements were made using the NeuroExplorer software package (MicroBrightfield). Dendritic morphology was used to identify cell type and layer. The tracing was aligned so the direction of the electric field traversed along the 90-degree line from the top of the tracing to the bottom. NeuroExplorer branched structure analyses were used to measure

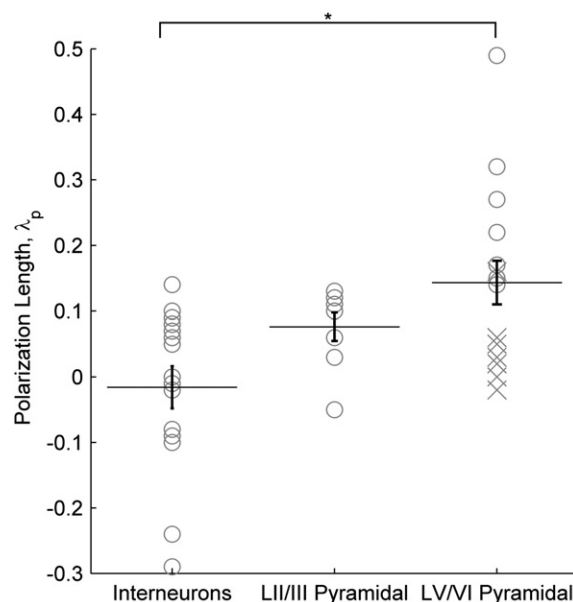


Figure 2 Cortical cell type polarization sensitivity. The polarization length, λ_p (mm), an indicator of mV of polarization per unit subthreshold electric field applied (mV/mm), is shown according to cell type. Asterisk denotes significant difference (t test) found between LV/VI pyramidal neurons and interneurons across layers. Points labeled as an “X” are neurons with cut dendritic trees that have still been included in all analyses (excluding these cells results in an additional significant difference between LII/III and LV/VI pyramids).

segment angle $\phi_{(seg)}$ and volume information for each segment of each individual neuron’s tracing.

Volume-weighted polar histogram generation

The volume of each segment was binned by segment angle in a polar histogram (Figure 4, A-C), and summarized by a single vector of mean angle (degrees) and vector strength (volume, μm^3). Ninety degrees is defined as pointing toward the anodal electric field stimulating electrode. Histograms were generated using the Matlab (Mathworks, Natick, Massachusetts) Circular Statistics Toolbox by Philip Berens.

DC stimulation strength-time to first spike curves

To determine respective stimulation “DC-chronaxies,” the threshold stimulation magnitude in response to incrementing electric field steps of 100-millisecond duration (functionally DC), as well as to incrementing 100-millisecond steps of somatic current injection, was plotted against the inverse of the time to first spike. These data were fit to the equation $S = S_o + S_o C/t$, where S is the threshold stimulation magnitude (in nanoampere for current injection, millivolt/millimeter for electric field stimulation), S_o is the rheobase corresponding to the horizontal asymptote of the

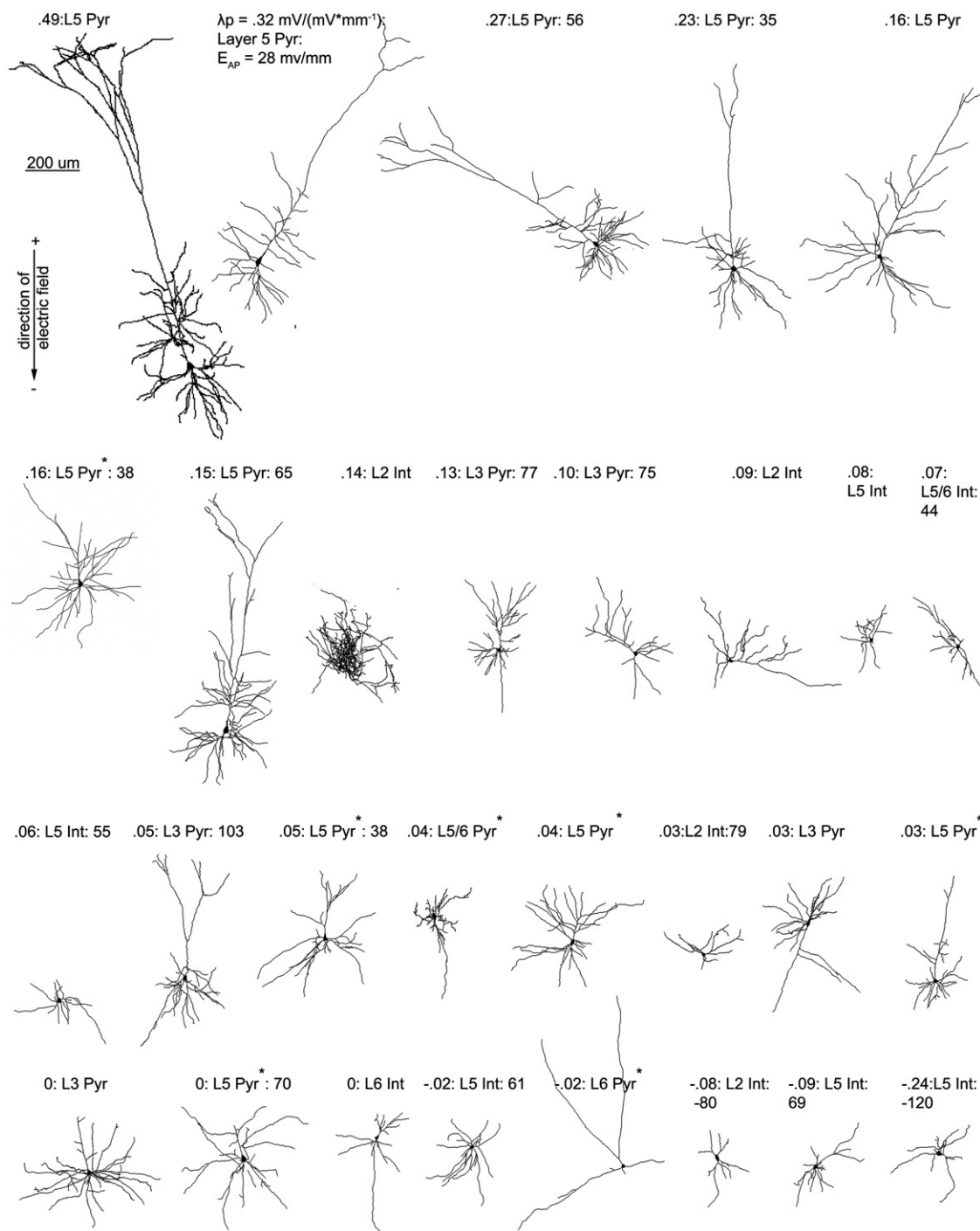


Figure 3 Cortical neuron morphologic reconstructions in decreasing order of electric field induced somatic subthreshold polarization sensitivity. Three items are listed for each cell, electric field induced somatic polarization length, λ_p (mm), an indicator of mV of polarization per unit electric field applied (mV/mm); layer and cell type (pyramidal or interneuron); and if tested for that cell, electric field induced firing threshold. An asterisk next to the label for cell type denotes a neuron with a presumably cut dendritic tree (slicing related change), that has still been included in all analyses.

strength-duration curve, C is the DC-chronaxie equal to the duration of stimulation pulse having twice the intensity of the rheobase, and t is time to first spike in milliseconds.⁶⁰ Note that “classic” strength duration curves are determined by using duration of incrementing stimulation pulse necessary to trigger an AP.⁶¹

Results

We quantified the acute effects of uniform electric fields on cortical neurons *in vitro*. For the cases of subthreshold and suprathreshold fields, we considered whether neuronal

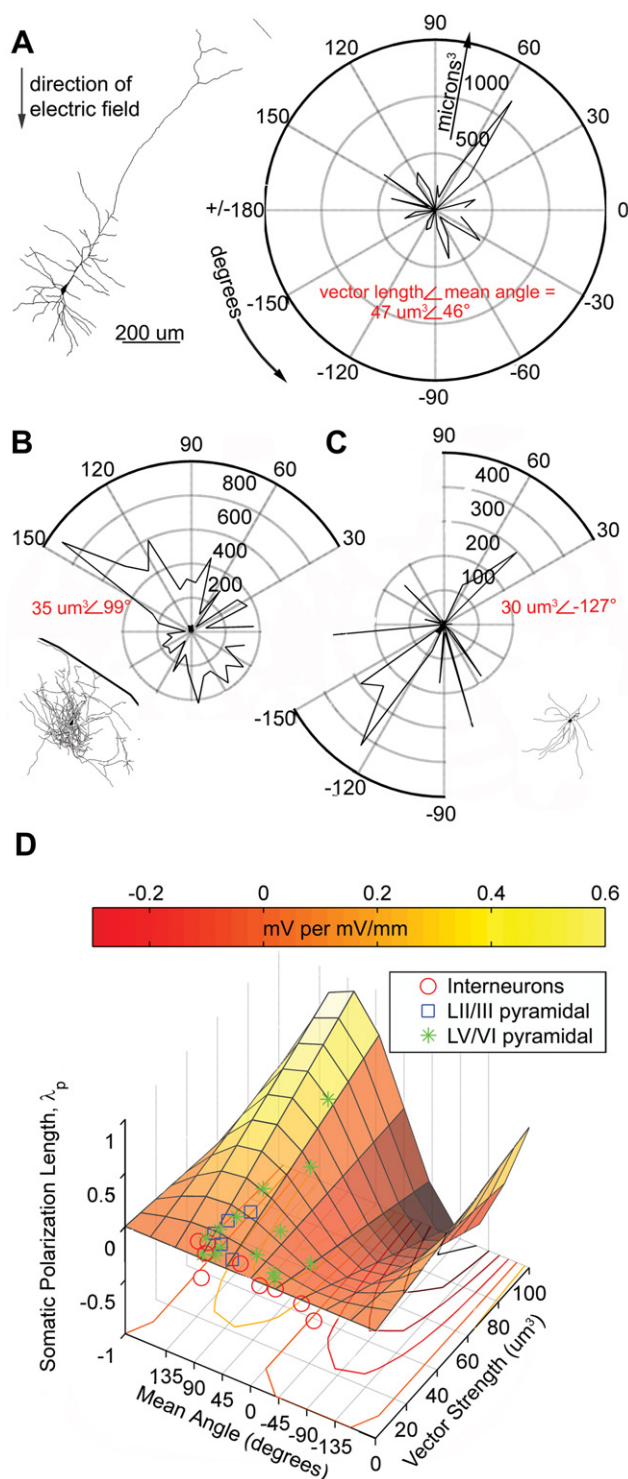


Figure 4 Polar histogram coherence vector: Neuronal morphology predicts somatic polarization sensitivity to subthreshold electric fields. **A–C**, Example tracings and corresponding volume weighted polar histograms of **(A)** LV regular spiking pyramidal neuron with electric field orientation. The polarization length, λ_p (mm), an indicator of mV of polarization per unit electric field applied (mV/mm), = 0.32 mm. The polar histogram can be summarized by the variables: mean angle = 46 degrees and vector strength = $47 \mu\text{m}^3$, representing the center of mass of the histogram; **(B)** LII fast spiking interneuron with

responses could be distinguished based on cortical cell type or neuronal morphology. Cortical cell types can be defined by anatomic and biophysical distinctions, while we developed a parsimonious metric of neuronal morphology relative to the orientation of applied uniform fields. In response to subthreshold fields, neuronal compartments polarize linearly with the amplitude of the applied electric field^{35,38,40–42}; for each neuron, somatic subthreshold sensitivity is defined by the polarization length constant: λ_p (in millimeters). Thus, for a given subthreshold electric field E (in millivolts/millimeters), neuronal soma will polarize $E\lambda_p$ mV. The sign of the polarization length reflects the polarity of polarization for a given electric field direction. Suprathreshold fields induce nonlinear responses in the cell membrane, including APs and/or EPSPs from activated afferents. The electric field threshold for triggering an AP in a given neuron reflects the neuron's specific sensitivity to suprathreshold fields. The main objective of this study was to determine whether subthreshold and suprathreshold sensitivities to electric fields could be correlated with cortical cell type or neuronal morphology.

Cortical cell subthreshold polarization in response to uniform electric fields

A total of 51 neurons from M1 were recorded, 37 of which were identified by cortical layer and cell type. Consistent with findings in other structures,^{23,25} the magnitude of cortical subthreshold somatic polarization increased linearly with increasing electric field steps, and reversed polarity with the direction of the applied electric field.

Per our convention (see the Methods section), a “positive” subthreshold soma polarization indicated a positive field (anode proximal to pial surface) resulting in somatic depolarization; whereas a “negative” subthreshold polarization indicates a positive field resulting in a somatic hyperpolarization. The polarity and polarization length (sensitivity) of each neuronal soma in response to an applied electric field was quantified.

Fifty-one cells had a subthreshold transmembrane polarization length, λ_p , ranging from 0.29 to 0.49 mm (such that field-induced subthreshold polarization = $\lambda_p \cdot E$ mV, where E is the applied electric field in units of millivolts/millimeters). The 14 identified layer V/VI (LV/VI) pyramidal cells had a range of polarization lengths, λ_p , from 0.03 to 0.49 mm. The eight identified layer II/III (LII/III) cells had

polarization length = 0.14 mm, mean angle = 99 degrees and vector strength = 0.14 mm ; and **(C)** LV fast spiking interneuron with polarization length = 0.02 mm, mean angle = 127 degrees and vector strength = $30 \mu\text{m}^3$. **D**, Summary plot of all neurons recorded and traced, with polar histogram coherence vectors as predictors of somatic polarization per electric field for each neuron. The colored plane is the statistically significant, best fit regression to the equation: polarization strength = $m \cdot \sin(\text{mean angle}) \cdot \text{vector strength}$ ($P < .02$, $r^2 = 0.41$, $n = 30$).

subthreshold polarization lengths, ranging from 0.05 to 0.13 mm. The 15 identified interneurons (from across all layers) had subthreshold polarization lengths ranging from 0.29 to 0.14 mm. These data are thus indicative of the range of possible subthreshold polarization values for a distributed population of cortical neurons. These polarization ranges are reported without accounting for variable cell angle relative to the electric field, and morphology differences within and across cell types^{51,62} (including slicing-related damage).

Without accounting for variable cell morphology relative to the electric field, a significant difference was found between the polarization length, λ_p , for interneurons across layers and LV/VI pyramidal neurons ($P < .02$), the difference between interneurons across layers and LII/III pyramidal neurons approached significance ($P = .06$) (*t* test, Figure 2), and were significantly higher than LII/III pyramidal neurons and interneurons across layers after rejecting cells damage due to slicing (marked with an “x” in Figure 2). Layer V neurons represented the seven highest (19%) individual somatic polarization values of the 37 identified cells (Figure 3).

Neuronal morphology relative to applied electric field correlates to induced subthreshold polarization: volume-weighted polar histograms

Volume-weighted polar histograms were constructed based on morphologic reconstructions of intracellularly recorded neurons (see the Methods section). This reduced representation of individual neuron morphology may be described by a mean angle and vector length (Figure 4, A-C). Mean angle and vector strength were significantly correlated to somatic polarization length, λ_p (Figure 4D, Supplementary Figure 2, regression model: $\lambda_p = m \cdot \sin(\text{mean angle})$ vector strength, for each neuron's mean angle, vector strength, and polarization length, where m represents a single scaling variable common to all neurons). The significantly fit plane illustrates the correlation between the asymmetry of neuronal morphology relative to the soma (vector strength), modulated by the sine of the mean angle of that morphologic projection relative to the electric field, with increasing polarization length (F -statistic = 19.52, $P < .001$, $r^2 = 0.41$, $n = 30$). Neuronal morphologies with mean angles of 0 or 180 degrees (ie, perpendicular to the electric field) would be represented in the model with polarization lengths of 0 mm [$\sin(0 \text{ degrees}) = \sin(180 \text{ degrees}) = 0$]. Mean angles of 90 or 270 degrees would be represented as the optimal orientation relative to the electric field to respectively depolarize or hyperpolarize the neuron [$\sin(90 \text{ degrees}) = 1$, $\sin(270 \text{ degrees}) = -1$]. Electric field-induced AP threshold did not correlate with mean angle and vector strength for our sampled cortical neuron population.

If all the neurons we recorded were optimally oriented to the electric field (mean angle = 90 degrees), the regression model would reduce to $\lambda_p \propto$ vector strength. A significant difference was found between the vector strength for interneurons across layers and both LII/III pyramids ($P < .001$)

as well as LV/VI pyramidal neurons ($P < .04$) (*t* test, Figure 5).

Cortical cell AP threshold in response to uniform electric fields

The minimum AP threshold in response to 100 milliseconds, \pm polarity electric field square pulses was determined ($n = 29$). Three cells were able to fire in both electric field polarities and the lesser magnitude polarity was considered the “minimum” threshold. Of 26 cells, 21 had a positive minimum threshold ranging from 28-101 mV/mm (mean = 58 ± 5 mV/mm), and two cells had negative minimum thresholds of 80 and 120 mV/mm (mean = 100 ± 20 mV/mm). Six cells did not fire an AP in response to the maximum electric field tested in either polarity. No cells fired in response to the offset of the electric field step (eg, in response to anodic break).

The minimum electric field induced firing threshold for identified LV/VI pyramidal cells ranged from 28-79 mV/mm ($n = 9$, mean = 57 ± 6 mV/mm). For LII/III pyramidal neurons, the minimum electric field AP threshold range was 70-104 mV/mm ($n = 6$, 81 ± 3 mV/mm). Thus, all identified pyramidal cells had a positive minimum AP threshold. The minimum electric field AP threshold range for interneurons was 44-79 mV/mm in the positive direction ($n = 6$, 68 ± 9 mV/mm), and 80 and 120 mV/mm in the negative direction ($n = 2$, 100 ± 20 mV/mm) (Supplementary Figure 3). A significant difference was found between the absolute value electric field firing threshold of LV/VI pyramidal neurons, and LII/III pyramids ($P < .002$) (*t* test, Figure 6). Note this difference was observed without accounting for variable cell angle relative to the electric field, morphology differences within and across cell types (and slicing-related damage), or presynaptic contribution.

Increasing intensity of electric field beyond the subthreshold polarization range (see the Methods section) resulted in EPSPs for most cells ($n = 26$) reflecting the activation of APs in axons afferent to the specific cortical neuron. This was in distinction to relatively rare EPSPs when electric field stimulation was off. In all but three of 29 tested neurons, EPSPs were observed in response to electric field pulses of lesser magnitude than AP threshold (Figure 7). For cells exhibiting EPSPs, the minimum positive electric field value inducing EPSPs ranged from 12-69 mV/mm (mean = 49 ± 4 mV/mm) ($n = 18$). The negative EPSP threshold range was 22 to 104 mV/mm (mean = 62 ± 7) ($n = 16$). These EPSPs were suppressed by bath application of glutamatergic transmission blockers CNQX and APV ($n = 4$, Figure 7) consistent with an orthodromic origin. After glutamatergic transmission blockade, APs could no longer be triggered in these four cells when stimulated up to the maximal intensity electric field tested (up to ± 79 -110 mV/mm). This analysis underscores the potential contribution of afferent glutamatergic synapses in depolarizing cells to AP threshold, in response to 100-millisecond electric field pulses.

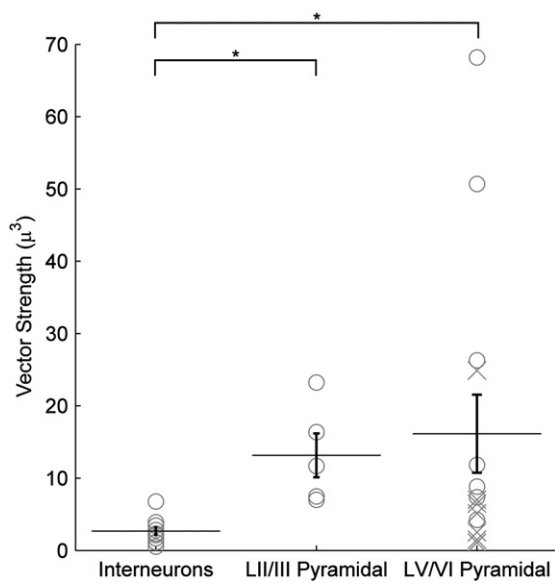


Figure 5 Cortical cell type vector strengths. The polar histogram (Figure 4) summary variable vector strength, is shown according to cell type. Asterisk denotes significant difference (t test) found between interneurons across layers and both LV/VI pyramidal neurons, as well as LII/III pyramidal neurons. Points labeled as an “X” are neurons with cut dendritic trees that have still been included in all analyses.

Stimulation parameters used in TMS and TES are typically short duration pulses less than 1 millisecond, and can be either monophasic or biphasic. As an initial characterization of the biophysics of cortical cell types in response to stimuli of brief duration, we tested the response of 19 cells to (0.5 millisecond) square wave electric field stimuli up to the intensity limits of our experimental setup (up to 79-120 mV/mm). Of 19 cells, two responded to a 0.5-millisecond square pulse step (mean = 88 ± 8 mV/mm); these cells responded to this 0.5-millisecond electric field stimuli with a spike approximately 2 milliseconds after stimulation onset; this short delay is indicative of direct neuronal activation (ie, the time course excludes synaptic contributions). EPSPs, reflecting orthodromic activation, were observed in another two cells at the maximum intensity tested (mean 100 ± 6 mV/mm). Thus, as expected, cortical AP threshold increases rapidly with decreasing pulse duration (see also DC-chronaxie discussed later in the text); We can conclude that electric field strengths greater than 79-120 mV/mm are necessary for significant activation of *quiescent* (see the Discussion section) cortical neurons in slice preparations by 0.5-millisecond (TMS-like) electric field pulses.

Differing mechanisms of AP initiation between intracellular current injection and suprathreshold electric field stimulation

In 10 of 26 cells, we observed a transition from regular spiking behavior in response to intracellular current

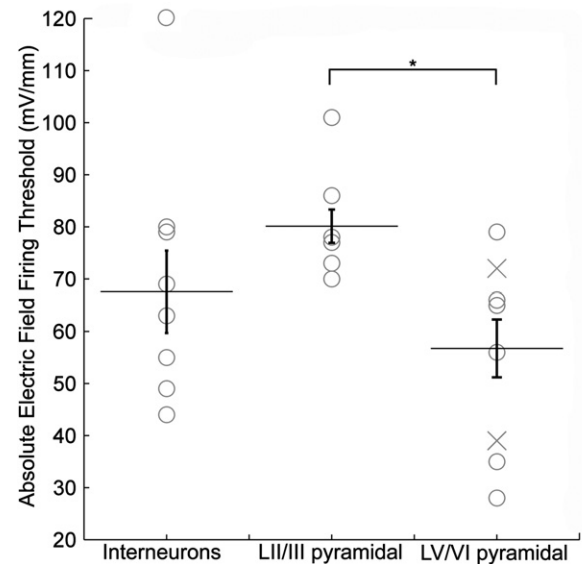


Figure 6 Cortical cell type electric field firing thresholds. The minimum absolute electric field firing threshold, in response to 100 millisecond incrementing electric field steps, is shown according to cell type. Asterisk denotes significant difference (t test) found between LV/VI pyramidal neurons, and LII/III pyramidal neurons.

injection, to intrinsic burst spiking (see the Methods section) when the same cell is stimulated by an electric field (Figure 8, A). Four of these cells were classified as LII/III pyramidal and six were classified as LV/VI pyramidal. These data indicate a change in the intrinsic firing pattern of cells, depending on the type of stimulation used.

The firing time of 26 cells in response to 100-millisecond incrementing steps of electric field and somatic current injection was compared. DC stimulation intensity time to first AP plots (eg, strength-duration curves) were constructed for each cell (see the Methods section), for both stimulation types (Figure 8, A). In 23 of 26 cells, the DC-chronaxie through electric field stimulation was lower than that of intracellular current injection, resulting in a significant difference between stimulation types (t test, $P < .01$, Figure 8, B). Eight of these cells were unable to be identified as a particular cell type. Among LV/VI cells, a significant difference between the DC-chronaxie of electric field stimulation and that of intracellular current injection was evident ($n = 8$, $P < .001$), whereas for LII/III cells ($n = 6$, $P = .09$) and for interneurons ($P = .07$, $n = 4$) the difference approached significance.

Discussion

To address the basic neural mechanisms of cortical electrotherapy, in this report we used *in vitro* whole-cell recordings and uniform electric field stimulation. A necessary step toward the rational design of subthreshold and suprathreshold brain stimulation paradigms is a systematic

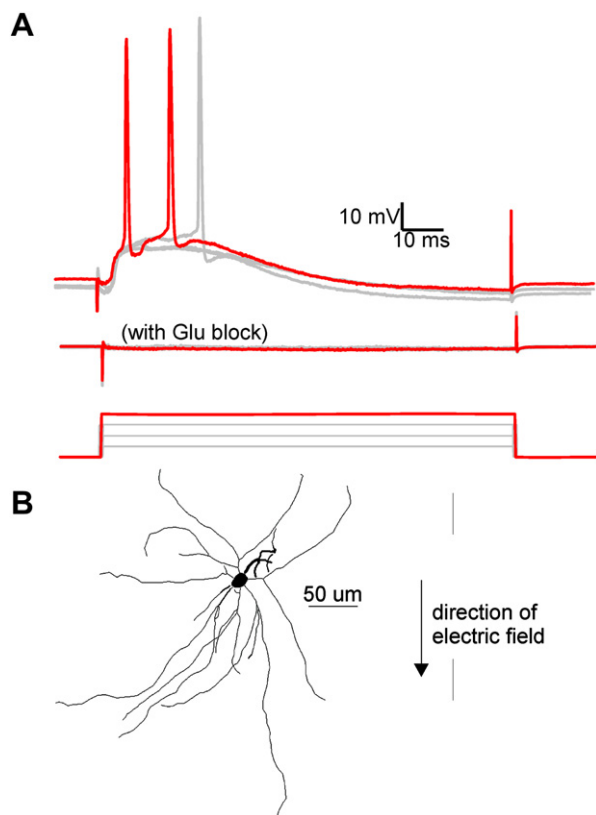


Figure 7 Electric field induced excitatory postsynaptic potentials are reduced by bath application of CNQX and APV. **A**, Overlay of the response to electric field steps of increasing intensity. Top: Recorded intracellular voltage response to electric field steps of 51, 57, 63, and 70 (red trace) mV/mm. Note 63 and 70 mV/mm electric field steps induced action potentials. Middle: Voltage response to the same field intensities after 15 minute bath application of 20 μ M CNQX and 50 μ M APV. Bottom: Applied electric field waveforms. **B**, Tracing of LV fast spiking interneuron described in **A**.

and quantitative method for predicting which neuronal elements respond to electric fields; this analysis can then be scaffolded onto theories of network processing and the ultimate therapeutic outcomes.

Relevance of *in vitro* data to clinical brain stimulation

Several factors concomitantly facilitate the precise characterization of electric field effects *in vitro*, while qualifying how *in vitro* data are used to understand and design clinical electrotherapies. The application of uniform electric fields to brain slice preparations^{25,26,39,48,52,54,55,63} results in each cell exposed to an identical “electrical environment,” such that differences in neuronal responses can be attributed (and correlated) directly to differences in neuronal morphologic/biophysical characteristics (Supplementary Figure 1). Only in cases in which electric fields induced in the brain are uniform on the scale of a single neuron, as may be the case

for noninvasive stimulation or distant cortical electrodes, can our data be used to directly predict neuronal response to the specific “quasiuniform” electric field at each location (eg, cortical column) in the brain.

In brain slices, the majority of afferents are cut, and intact synapses are inactive compared with the *in vivo* situation.^{51,62} These changes affect cellular properties such as resting membrane potential and conductance, as well as AP threshold. Similarly, spontaneous network oscillations, and other forms of “tonic” system drive, which may modulate neuronal subthreshold and suprathreshold response,^{64,65} are absent in brain slices superfused with “normal” ACSF.

In response to subthreshold stimulation, in the absence of (by definition) electric field-induced synaptic activation, and ongoing neuronal oscillations (*in vitro*), neuronal morphology merits investigation as a predictor of neuronal response. Our morphologic reconstructions account for, in part, the inherent cutting of some dendritic processes during brain slice preparation.

Suprathreshold responses integrate the direct neuronal response to the electric field and the cumulative synaptic response by the network. Thus cell type, encompassing laminar position, network connectivity, and neuronal morphology merits investigation.

Response to subthreshold fields

It is well established, that in response to subthreshold electric fields, neurons polarize in a compartment specific fashion with compartments oriented toward the anode generally hyperpolarizing and compartments oriented toward the cathode depolarizing.^{21,25,26,54,63,66} Somatic polarization may be reflected as a corresponding change in spontaneous firing rate.^{24,27,67} Neuronal cell types with a nonsymmetric dendritic morphology are preferentially modulated by the electric field.^{23,24}

Our results indicate that based only on volume-weighted neuronal morphology (without considering cell/compartment specific membrane biophysics) the polarity of cortical neuron somatic membrane polarization by uniform fields can be predicted with high fidelity, and the magnitude of polarization approximated, using the volume-weighted polar histogram coherence vector (described by the mean angle and vector length).

The polar histogram coherence vectors provide a parsimonious model of cortical neuron morphology in relation to electric field-induced somatic polarization. Its intuitive applicability, independence of nonlinear cellular biophysics, and lower computational overhead gives it merit. This intuitive approach is thus applicable to predict subthreshold polarization from morphologic data. For example, because the vector strength is lower for symmetric cells (eg, some interneurons; Figure 5), the polar histogram model predicts reduced maximum somatic polarization length (λ_p) for such cells compared with larger, more asymmetric (e.g., pyramidal) cells with a higher vector strength. The model

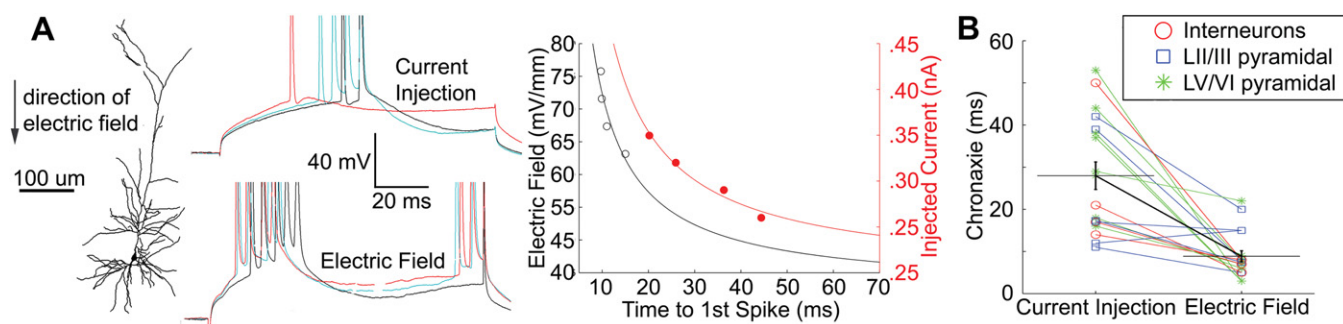


Figure 8 Time to first spike strength of stimulation chronaxie measurements are lower for electric field stimulation than somatic intracellular current injection. **A**, Example morphologic reconstruction of a LV intrinsic bursting pyramidal neuron with transmembrane polarization in response to successive steps of intracellular current injection (*top*), and electric field stimulation (*bottom*). Note modulation of firing pattern from regular spiking (*top*, current injection), to intrinsic bursting (*bottom*, field stimulation). Summary plot (right), of the time to first spike in response to electric field stimulation (left axis, black) and injected current (right axis, red). The solid lines are best fit curves to $y = 1/(\text{time to first spike})$. **B**, Comparison of chronaxies, for current injection and electric field stimulation, for each recorded neuron. Statistically significant difference ($P < .01$) between stimulation methods for all cells.

also predicts that optimal positive and negative polarization length, for any given cell, is achieved for mean angles of 90 and 270 degrees, respectively, aligned with the electric fields. Cells with mean angles perpendicular to the direction of the electric field (0 or 180 degrees) are predicted not to polarize significantly (low λ_p), regardless of vector strength.

However, the polar histogram coherence vector model neglects weighting of neuronal segments by their proximity to the soma and distributed cellular biophysics. Indeed, though the dependence of the observed polarization on polar histogram morphologic variables is significant ($P < .001$) this parsimonious model does not account for almost half of the observed variance ($r^2 = 0.41$). Given compartment specific biophysical parameters for each neuron, the second derivative of the extracellular voltage along the membrane (i.e., activating function)^{40,68} would yield more accurate predications (morphologic data shall be published on (<http://www.neuromorpho.org>)).

Individually, layer V pyramids exhibited the highest measured somatic sensitivities to subthreshold fields (polarization lengths, λ_p), and the highest polar histogram vector strengths, a measure of the asymmetry of the volume of neuronal membrane in relation to the soma. Applied subthreshold electric field therapies (tDCS, tACS), if quasi-uniform across cortical regions, would thus preferentially polarize layer V cell somas. Human cortical neurons can be longer than the rat cortical neurons investigated here.⁶² However, assuming the ratio of volume between the sum of apical and basal neuronal elements is similar between rat and human cortical neurons, then despite differences in overall size the polar histogram metric would scale according to size, to predict a similar distribution of somatic polarization differences across species (Figure 2).

Distal terminal electric field induced polarization is important to quantify because: (a) the maximum polarization is thought to occur at the terminals,^{21,23,38} and (b) dendrite polarization will modulate neuronal processing (eg, the site of synaptic input).²⁵ The distal polarization

of a symmetrically branching dendritic tree has been modeled,³⁸ in one case with approximately 2.5 times greater polarization at the distal terminal than at the soma.³⁷ We emphasize that basal and apical dendrites will concomitantly polarize in opposite directions (Supplemental Figure 1), thus it is incorrect to describe any electric field (experimentally or clinically) as globally depolarizing or hyperpolarizing.

Response to suprathreshold fields

Several lines of evidence suggest that AP initiation in response to uniform electric fields cannot be explained by a simple linear depolarization of the soma to threshold: (1) although the values of subthreshold polarization per unit electric field recorded at the soma linearly correlated to field polarity, in some cells, spiking was initiated with fields of either polarity, or of polarity opposite to the subthreshold polarization value; (2) the values of subthreshold polarization per unit electric field recorded at the soma, multiplied by the electric field-induced firing threshold (expected somatic polarization at threshold electric field) is less than the difference between resting membrane potential and AP threshold (expected somatic polarization necessary for somatic AP initiation); an extreme example was a cell with a subthreshold somatic polarization value of 0 mV*(mV/mm)⁻¹ and electric field firing threshold of 72 mV/mm; (3) EPSPs were evident in most cells recorded during stimulation and were dependent on glutamatergic synaptic activity; and (4) the DC chronaxie values for electric field stimulation were lower than for intracellular current injection reflecting differing neuronal elements triggering AP initiation for the two stimulation cases,⁶⁰ and/or synaptic contributions toward electric field-induced firing threshold. The spatial profile of stimulation may also impact chronaxie measurements; with neuronal elements charging and summing in parallel during uniform electric

field stimulation. Related to this latter point, (5) some cells that were not categorized as “intrinsically bursting” in response to intracellular current injection (see the Methods section), exhibited bursting behavior when stimulated by electric fields.

Bursting has been hypothesized as dependent on the removal of inactivation of hyperpolarization-gated channels of a distal dendritic region (e.g., by inhibitory inputs), whereas an AP generated in a depolarized region of the cell back-propagates to this distal hyperpolarized region resulting in dendritic calcium spikes.⁶⁹⁻⁷¹ The original AP and subsequent dendritic spikes may be observed from a somatic recording as a burst response. In contrast to intracellular current injection, electric fields simultaneously depolarize and hyperpolarize distinct neuronal compartments (Supplementary Figure 1). This may be a mechanism for the observed modulation to bursting in response to the electric field. We have observed modulation of firing to a burst response in pyramidal cells, in which distal and basal compartments are electrotonically distant.⁷²

In coronal *in vitro* brain slices, individual LV/VI cells demonstrated the lowest AP threshold in responses to 100-millisecond uniform electric fields. We have found evidence for both direct and orthodromic activation of LV/VI cells. However, it is important to emphasize that recruitment order is a spectrum across cell types, consistent with a network/orthodromic contribution to activation for most cells. One goal of probing cortical slices with suprathreshold electric fields is to characterize the use of cortical brain slices as a research tool for suprathreshold noninvasive transcranial stimulation (eg, TMS). We have recorded a sparse sample of cortical neurons, with three of 29 cells exhibiting direct activation (without EPSPs) in response to 100-millisecond pulses, the majority of cells fired through a summation of EPSPs and field-induced polarization. An unrelated minority of cells responded to short, TMS-like pulses, in which the electric field is turned off before the time for synaptic transmission (precluding summation of EPSPs and field-polarization). Lower stimulator outputs of lateral medial (l-m) TMS coil orientations or any stimulator outputs of posterior-anterior (p-a) TMS are considered only to induce (indirect) i-waves, whereas greater stimulator output in the l-m orientation is necessary to induce (direct) d-waves.^{73,74}

Despite experimental differences between *in vitro* uniform electric fields and human cranial stimulation, biophysical features governing suprathreshold response (e.g., morphology, cell type, connectivity) should be generalizable. *In vitro*, because all neurons were exposed to a uniform electric field, we demonstrated that differences in suprathreshold response can be attributed to (the uncontrolled variable of) biophysical distinctions of cortical cell types.

In addition, the absolute firing thresholds and recruitment order *in vitro* may be different than during clinical stimulation because of: (1) greater electric field nonuniformities during clinical stimulation, particularly the action

potential initiation zone; (2) using *in vitro* preparations, portions of axons are inevitably cut, including corticospinal axons, that have been attributed to d-waves^{19,75} and cortico-cortical afferents linked to the generation of i-waves^{74,76}; (3) the square pulse used here leading to differing neuronal activation than the monophasic or biphasic waveforms generated by TMS,⁷⁷ whereas the pulse lengths used in TMS and TES are much shorter as well; (4) differences in size, length constant, and morphology between human and rat cortical neurons; and (5) ongoing network activity (e.g., state dependent activation).

For the reasons noted above, *in vitro*, only a minority of neurons fired in response to 500 μ s electric field step pulses with amplitudes up to the maximum possible for our experimental setup, which encompasses the reported range of clinical TMS motor-evoked potential (MEP) threshold amplitudes of 30-130 mV/mm.⁷⁸⁻⁸⁰ In addition, the observed recruitment orders across cortical cell types in response to 100-millisecond square pulses, may not hold for sub-500 μ s pulses, possibly because at this timescale summation of direct electric field polarization and (delayed) EPSP-induced polarization is not possible. In addition, the capacitance of differing cortical cell types/cellular compartments may change polarization induced by electric fields of varying pulse lengths.^{81,82}

Toward a mechanistic understanding and rational design of clinical cortical brain stimulation

Which neuronal elements are activated by electrical stimulation are considered to underlie the ultimate behavioral and therapeutic outcomes.²⁹ Central to this idea is that not all neurons will be equally effected by a given stimulation protocol, and that distinct stimulation protocols target distinct neuronal populations/neuronal compartments. Therefore, determining which cells are acutely modulated by stimulation is a pivotal first step toward the rational design of electrotherapies; however, this is only a first step toward the complex analysis of how electrical stimulation affects information processing, synaptic plasticity, network function and ultimately behavior. Conversely, network activity may affect both subthreshold polarization sensitivity (polarization length, λ_p) and suprathreshold recruitment order. The current study addressed only the first step by taking advantage of the isolated brain slice preparation.

Development of subthreshold stimulation paradigms should consider the polarization of specific neuronal compartments (such as the soma or specific dendritic terminals), in the context of their roles in ongoing neuronal processing. For the range of electric fields induced by typical subthreshold clinical electrotherapies (eg, tDCS), the predicted membrane polarization is on the order of millivolts; even at the tufts of the largest cortical neurons.³⁷ How can such relatively small polarizations lead to significant functional changes in the brain? When considered in

the context of ongoing activity, we have shown that acutely, weak fields may be amplified at the single cell⁴⁸ and network⁶⁵ levels, through changes in spike timing. In addition to these acute “amplification” mechanisms, it is necessary to characterize the plastic effects of electrical stimulation protocols; for example, prolonged weak depolarization (>10 minutes), is thought to lead to plastic changes as observed during tDCS.⁸³⁻⁸⁵

The ultimate goal of rational electrotherapy is to promote changes in network function that alleviate behavioral symptoms while minimizing disruption of cognitive function. The characterization of cellular responses to stimulation is a necessary but incremental step toward this goal. In summary, the current study addresses the importance of cortical neuronal morphology and cortical cell type during subthreshold and suprathreshold electric field stimulation. These data are a necessary step toward a mechanistic understanding of clinical cortical electrotherapy, and the design of more targeted (eg, focal, fewer side effects, longer lasting) brain stimulation strategies.

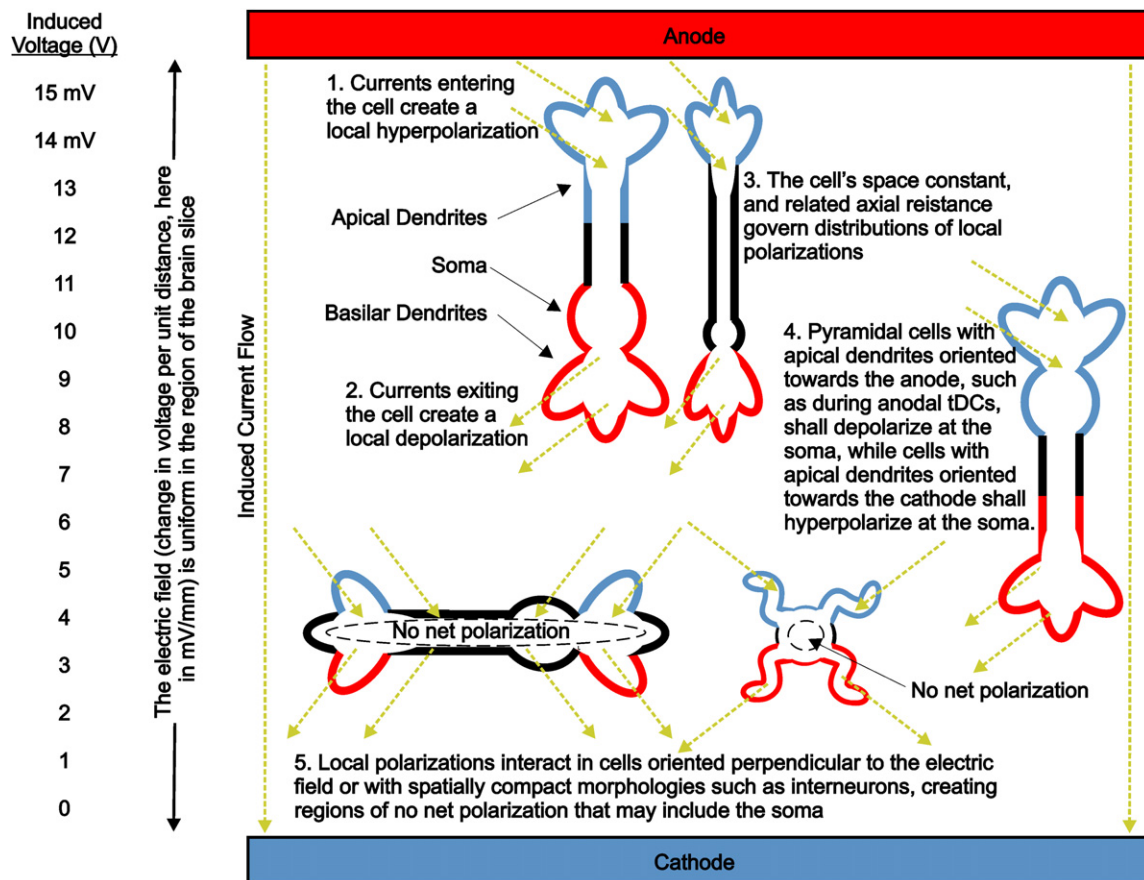
We acknowledge the following for their assistance: Abhishek Datta, Davide Reato, Reem Khalil, Jonathan B. Levitt, and Lucas C. Parra of the City College of New York; Zhi-De Deng, Angel V. Peterchev, Sébastien J. Thuaud and Stephen A. Siegelbaum of Columbia University, Boris Heifets and Pablo Castillo of Albert Einstein College of Medicine of Yeshiva University; Natascia Vedovato and David C. Gadsby of Rockefeller University; Jimmy K. Duong of the Irving Institute Biostatistics Consultation Service; Adair Oesterle of Sutter Instruments.

References

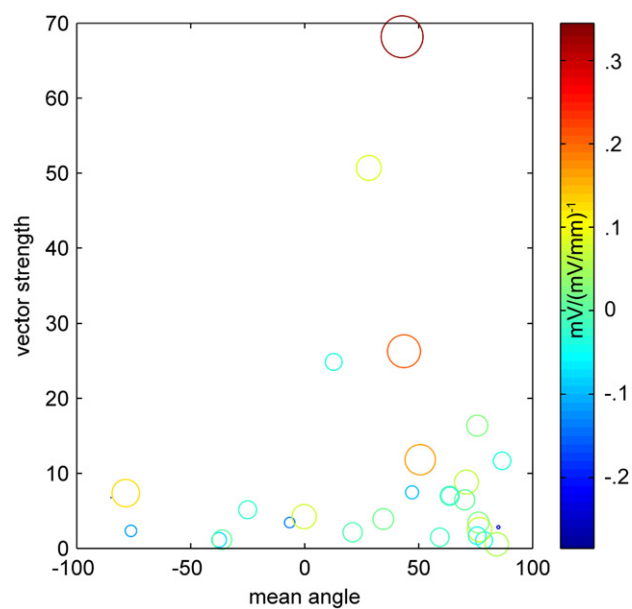
- Liebetanz D, Klinker F, Hering D, et al. Anticonvulsant effects of transcranial direct current stimulation (tDCS) in the rat cortical ramp model of focal epilepsy. *Epilepsia* 2006;47(7):1216-1224.
- George MS, Lisanby SH, Sackeim HA. Transcranial magnetic stimulation: applications in neuropsychiatry. *Arch Gen Psychiatry* 1999;56(4):300-311.
- Avery DH, Holtzheimer PE 3rd, Fawaz W, et al. A controlled study of repetitive transcranial magnetic stimulation in medication resistant major depression. *Biol Psychiatry* 2006;59(2):187-194.
- Boggio PS, Ferrucci R, Rigonatti SP, et al. Effects of transcranial direct current stimulation on working memory in patients with Parkinson's disease. *J Neurol Sci* 2006;249(1):31-38.
- Webster BR, Celnik PA, Cohen LG. Noninvasive brain stimulation in stroke rehabilitation. *NeuroRx* 2006;3(4):474-481.
- Fregni F, Boggio PS, Lima MC, et al. A sham controlled, phase II trial of transcranial direct current stimulation for the treatment of central pain in traumatic spinal cord injury. *Pain* 2006;122(1-2):197-209.
- Uy J, Ridding MC. Increased cortical excitability induced by transcranial DC and peripheral nerve stimulation. *J Neurosci Methods* 2003;127(2):193-197.
- Marshall L, Helgadottir H, Molle M, Born J. Boosting slow oscillations during sleep potentiates memory. *Nature* 2006;444(7119):610-613.
- Fregni F, Boggio PS, Nitsche M, et al. Anodal transcranial direct current stimulation of prefrontal cortex enhances working memory. *Exp Brain Res* 2005;166(1):23-30.
- Kincses TZ, Antal A, Nitsche NA, Bartfai O, Paulus W. Facilitation of probabilistic classification learning by transcranial direct current stimulation of the prefrontal cortex in the human. *Neuropsychologia* 2004;42(1):113-117.
- Amassian VE, Eberle L, Maccabee PJ, Cracco RQ. Modelling magnetic coil excitation of human cerebral cortex with a peripheral nerve immersed in a brain shaped volume conductor: the significance of fiber bending in excitation. *Electroencephalogr Clin Neurophysiol* 1992;85(5):291-301.
- Miranda PC, Lomarev M, Hallett M. Modeling the current distribution during transcranial direct current stimulation. *Clin Neurophysiol* 2006;117(7):1623-1629.
- Krings T, Buchbinder BR, Butler WE, et al. Functional magnetic resonance imaging and transcranial magnetic stimulation: complementary approaches in the evaluation of cortical motor function. *Neurology* 1997;48(5):1406-1416.
- Wassermann EM, Wang B, Zeffiro TA, et al. Locating the motor cortex on the MRI with transcranial magnetic stimulation and PET. *Neuroimage* 1996;3(1):1-9.
- Komssi S, Savolainen P, Heiskala J, Kahkonen S. Excitation threshold of the motor cortex estimated with transcranial magnetic stimulation electroencephalography. *Neuroreport* 2007;18(1):13-16.
- Normann RA, Maynard EM, Rousche PJ, Warren DJ. A neural interface for a cortical vision prosthesis. *Vision Res* 1999;39(15):2577-2587.
- Badi AN, Hillman T, Shelton C, Normann RA. A technique for implantation of a 3 dimensional penetrating electrode array in the modiolar nerve of cats and humans. *Arch Otolaryngol Head Neck Surg* 2002;128(9):1019-1025.
- Esser SK, Hill SL, Tononi G. Modeling the effects of transcranial magnetic stimulation on cortical circuits. *J Neurophysiol* 2005;94(1):622-639.
- Pascual Leone A, Valls-Sole J, Wassermann EM, Hallett M. Responses to rapid rate transcranial magnetic stimulation of the human motor cortex. *Brain* 1994;117(Pt 4):847-858.
- Takano B, Drzezga A, Peller M, et al. Short term modulation of regional excitability and blood flow in human motor cortex following rapid rate transcranial magnetic stimulation. *Neuroimage* 2004;23(3):849-859.
- Maccabee PJ, Amassian VE, Eberle LP, Cracco RQ. Magnetic coil stimulation of straight and bent amphibian and mammalian peripheral nerve in vitro: locus of excitation. *J Physiol* 1993;460:201-219.
- Amassian VE, Maccabee PJ, Cracco RQ, et al. The polarity of the induced electric field influences magnetic coil inhibition of human visual cortex: implications for the site of excitation. *Electroencephalogr Clin Neurophysiol* 1994;93(1):21-26.
- Chan CY, Hounsgaard J, Nicholson C. Effects of electric fields on transmembrane potential and excitability of turtle cerebellar Purkinje cells in vitro. *J Physiol* 1988;402:751-771.
- Hern JE, Landgren S, Phillips CG, Procter R. Selective excitation of corticofugal neurones by surface anodal stimulation of the baboon's motor cortex. *J Physiol* 1962;161:73-90.
- Bikson M, Inoue M, Akiyama H, et al. Effects of uniform extracellular DC electric fields on excitability in rat hippocampal slices in vitro. *J Physiol* 2004;557(Pt 1):175-190.
- Chan CY, Nicholson C. Modulation by applied electric fields of Purkinje and stellate cell activity in the isolated turtle cerebellum. *J Physiol* 1986;371:89-114.
- Purpura DP, McMurtry JG. Intracellular activities and evoked potential changes during polarization of motor cortex. *J Neurophysiol* 1965;28:166-185.
- Lopez L, Chan CY, Okada YC, Nicholson C. Multimodal characterization of population responses evoked by applied electric field in vitro: extracellular potential, magnetic evoked field, transmembrane potential, and current source density analysis. *J Neurosci* 1991;11(7):1998-2010.
- Ranck JB Jr. Which elements are excited in electrical stimulation of mammalian central nervous system: a review. *Brain Res* 1975;98(3):417-440.
- Wagner T, Valero-Cabré A, Pascual-Leone A. Noninvasive human brain stimulation. *Annu Rev Biomed Eng* 2007;9:527-565.

31. Gatter KC, Sloper JJ, Powell TP. The intrinsic connections of the cortex of area 4 of the monkey. *Brain* 1978;101(3):513 541.
32. Miranda PC, Hallett M, Basser PJ. The electric field induced in the brain by magnetic stimulation: a 3 D finite element analysis of the effect of tissue heterogeneity and anisotropy. *IEEE Trans Biomed Eng* 2003;50(9):1074 1085.
33. Wagner T, Fregni F, Fecteau S, Grodzinsky A, Zahn M, Pascual Leone A. Transcranial direct current stimulation: a computer based human model study. *Neuroimage* 2007;35(3):1113 1124.
34. Datta A, Elwassif M, Battaglia F, Bikson M. Transcranial current stimulation focality using disc and ring electrode configurations: FEM analysis. *J Neural Eng* 2008;5(2):163 174.
35. Rattay F. Analysis of models for extracellular fiber stimulation. *IEEE Trans Biomed Eng* 1989;36(7):676 682.
36. Nagarajan SS, Durand DM, Warman EN. Effects of induced electric fields on finite neuronal structures: a simulation study. *IEEE Trans Biomed Eng* 1993;40(11):1175 1188.
37. Hause L. A mathematical model for transmembrane potentials secondary to extracellular fields. In: Sances J, Larson S, editors. *Electroanaesthesia: biomedical and biophysical studies*. New York: Academic; 1975. p. 176 200.
38. Tranchina D, Nicholson C. A model for the polarization of neurons by extrinsically applied electric fields. *Biophys J* 1986;50(6):1139 1156.
39. Svirskis G, Baginskas A, Hounsgaard J, Gutman A. Electrotonic measurements by electric field induced polarization in neurons: theory and experimental estimation. *Biophys J* 1997;73(6):3004 3015.
40. McIntyre CC, Grill WM. Excitation of central nervous system neurons by nonuniform electric fields. *Biophys J* 1999;76(2):878 888.
41. Plonsey R, Barr RC. Electric field stimulation of excitable tissue. *IEEE Eng Med Biol Mag* 1998;17(5):130 137.
42. Plonsey R, Altman KW. Electrical stimulation of excitable cells a model approach. *Proc IEEE* 1988;76(9):1122 1129.
43. Rotem A, Moses E. Magnetic stimulation of one dimensional neuronal cultures. *Biophys J* 2008;94(12):5065 5078.
44. Valero Cabre A, Payne BR, Rushmore J, Lomber SG, Pascual Leone A. Impact of repetitive transcranial magnetic stimulation of the parietal cortex on metabolic brain activity: a 14C 2DG tracing study in the cat. *Exp Brain Res* 2005;163(1):1 12.
45. Durand DM. Suppression and control of epileptiform activity by electrical stimulation: a review. *Proc IEEE* 2001;89:1065 1082.
46. Roth BJ. Mechanisms for electrical stimulation of excitable tissue. *Crit Rev Biomed Eng* 1994;22(3 4):253 305.
47. Brumberg JC, Nowak LG, McCormick DA. Ionic mechanisms underlying repetitive high frequency burst firing in supragranular cortical neurons. *J Neurosci* 2000;20(13):4829 4843.
48. Radman T, Su Y, An JH, Parra LC, Bikson M. Spike timing amplifies the effect of electric fields on neurons: implications for endogenous field effects. *J Neurosci* 2007;27(11):3030 3036.
49. Ramos RL, Tam DM, Brumberg JC. Physiology and morphology of callosal projection neurons in mouse. *Neuroscience* 2008;153(3):654 663.
50. Yang CR, Seamans JK, Gorelova N. Electrophysiological and morphological properties of layers V VI principal pyramidal cells in rat prefrontal cortex in vitro. *J Neurosci* 1996;16(5):1904 1921.
51. McCormick DA, Connors BW, Lighthall JW, Prince DA. Comparative electrophysiology of pyramidal and sparsely spiny stellate neurons of the neocortex. *J Neurophysiol* 1985;54(4):782 806.
52. Deans JK, Powell AD, Jefferys JG. Sensitivity of coherent oscillations in rat hippocampus to AC electric fields. *J Physiol* 2007;583(Pt 2):555 565.
53. Ghai RS, Bikson K, Durand DM. Effects of applied electric fields on low calcium epileptiform activity in the CA1 region of rat hippocampal slices. *J Neurophysiol* 2000;84(1):274 280.
54. Francis JT, Gluckman BJ, Schiff SJ. Sensitivity of neurons to weak electric fields. *J Neurosci* 2003;23(19):7255 7261.
55. Gluckman BJ, Neel EJ, Netoff TI, Ditto WL, Spano ML, Schiff SJ. Electric field suppression of epileptiform activity in hippocampal slices. *J Neurophysiol* 1996;76(6):4202 4205.
56. Gluckman BJ, Nguyen H, Weinstein SL, Schiff SJ. Adaptive electric field control of epileptic seizures. *J Neurosci* 2001;21(2):590 600.
57. Brumberg JC, Hamzei Sichani F, Yuste R. Morphological and physiological characterization of layer VI corticofugal neurons of mouse primary visual cortex. *J Neurophysiol* 2003;89(5):2854 2867.
58. Rocco MM, Brumberg JC. The sensorimotor slice. *J Neurosci Methods* 2007;162(1 2):139 147.
59. Ramos RL, Smith PT, DeCola C, Tam D, Corzo O, Brumberg JC. Cytoarchitecture and transcriptional profiles of neocortical malformations in inbred mice. *Cereb Cortex* 2008;18(11):2614 2628.
60. Nowak LG, Bullier J. Axons, but not cell bodies, are activated by electrical stimulation in cortical gray matter. I. Evidence from chronaxie measurements. *Exp Brain Res* 1998;118(4):477 488.
61. Bostock H. The strength duration relationship for excitation of myelinated nerve: computed dependence on membrane parameters. *J Physiol* 1983;341:59 74.
62. Meyer G. Forms and spatial arrangement of neurons in the primary motor cortex of man. *J Comp Neurol* 1987;262(3):402 428.
63. Jefferys JG. Influence of electric fields on the excitability of granule cells in guinea pig hippocampal slices. *J Physiol* 1981;319:143 152.
64. Lakatos P, Shah AS, Knuth KH, Ulbert I, Karmos G, Schroeder CE. An oscillatory hierarchy controlling neuronal excitability and stimulus processing in the auditory cortex. *J Neurophysiol* 2005;94(3):1904 1911.
65. Parra LC, Bikson M. Model of the effect of extracellular fields on spike time coherence. *Conf Proc IEEE Eng Med Biol Soc* 2004;6:4584 4587.
66. Delgado Lezama R, Perrier JF, Hounsgaard J. Local facilitation of plateau potentials in dendrites of turtle motoneurons by synaptic activation of metabotropic receptors. *J Physiol* 1999;515(Pt 1):203 207.
67. Terzuolo CA, Bullock TH. Measurement of imposed voltage gradient adequate to modulate neuronal firing. *Proc Natl Acad Sci U S A* 1956;42(9):687 694.
68. McIntyre CC, Grill WM. Selective microstimulation of central nervous system neurons. *Ann Biomed Eng* 2000;28(3):219 233.
69. Izhikevich E. *Dynamical systems in neuroscience: geometry of excitability and bursting*. Cambridge (MA): MIT Press; 2005.
70. Lesica NA, Stanley GB. Encoding of natural scene movies by tonic and burst spikes in the lateral geniculate nucleus. *J Neurosci* 2004;24(47):10731 10740.
71. Lu SM, Guido W, Sherman SM. Effects of membrane voltage on receptive field properties of lateral geniculate neurons in the cat: contributions of the low threshold Ca²⁺ conductance. *J Neurophysiol* 1992;68(6):2185 2198.
72. Larkman AU, Major G, Stratford KJ, Jack JJ. Dendritic morphology of pyramidal neurones of the visual cortex of the rat: IV, electrical geometry. *J Comp Neurol* 1992;323(2):137 152.
73. Brocke J, Irlbacher K, Hauptmann B, Voss M, Brandt SA. Transcranial magnetic and electrical stimulation compared: does TES activate intracortical neuronal circuits? *Clin Neurophysiol* 2005;116(12):2748 2756.
74. Patton HD, Amassian VE. Single and multiple unit analysis of cortical stage of pyramidal tract activation. *J Neurophysiol* 1954;17(4):345 363.
75. Rothwell J, Burke D, Hicks R, Stephen J, Woodforth I, Crawford M. Transcranial electrical stimulation of the motor cortex in man: further evidence for the site of activation. *J Physiol* 1994;481(Pt 1):243 250.
76. Nakamura H, Kitigawa H, Kawaguchi Y, Tsuji H. Intracortical facilitation and inhibition after transcranial magnetic stimulation in conscious humans. *J Physiol* 1997;498(Pt 3):817 823.
77. Sommer M, Lang N, Tergau F, Paulus W. Neuronal tissue polarization induced by repetitive transcranial magnetic stimulation? *Neuroreport* 2002;13(6):809 811.
78. Epstein CM, Schwartzberg DG, Davey KR, Sudderth DB. Localizing the site of magnetic brain stimulation in humans. *Neurology* 1990;40(4):666 670.

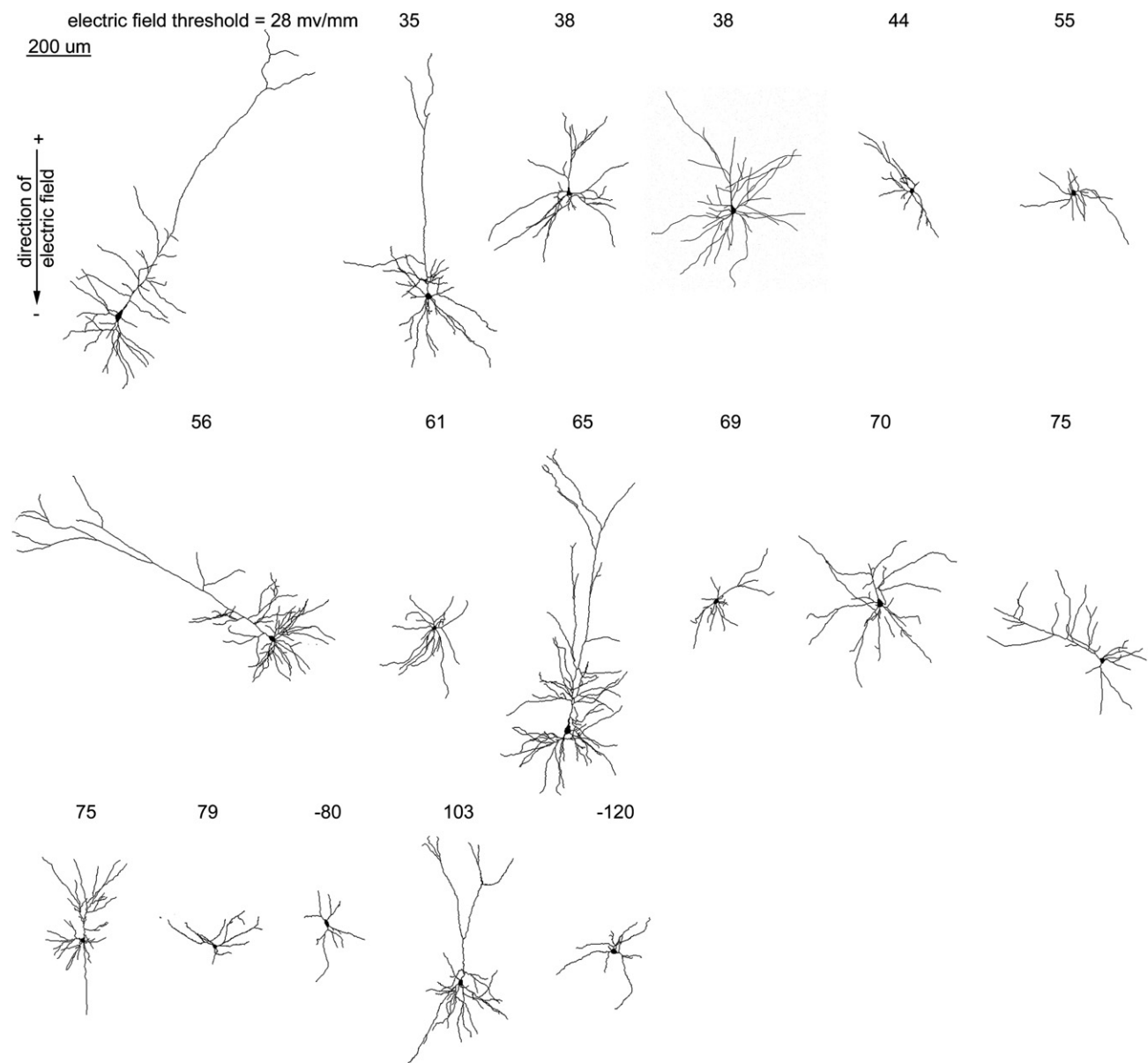
79. Rudiak D, Marg E. Finding the depth of magnetic brain stimulation: a re evaluation. *Electroencephalogr Clin Neurophysiol* 1994;93(5):358 371.
80. Thielscher A, Kammer T. Linking physics with physiology in TMS: a sphere field model to determine the cortical stimulation site in TMS. *Neuroimage* 2002;17(3):1117 1130.
81. Peterchev AV, Jalinous R, Lisanby SH. A transcranial magnetic stimulator inducing near rectangular pulses with controllable pulse width (cTMS). *IEEE Trans Biomed Eng* 2008;55(1):257 266.
82. Tehovnik EJ, Tolias AS, Sultan F, Slocum WM, Logothetis NK. Direct and indirect activation of cortical neurons by electrical microstimulation. *J Neurophysiol* 2006;96(2):512 521.
83. Nitsche MA, Liebetanz D, Antal A, Lang N, Tergau F, Paulus W. Modulation of cortical excitability by weak direct current stimulation—technical, safety and functional aspects. *Suppl Clin Neurophysiol* 2003;56:255 276.
84. Nitsche MA, Fricke K, Henschke U, et al. Pharmacological modulation of cortical excitability shifts induced by transcranial direct current stimulation in humans. *J Physiol* 2003;553(Pt 1):293 301.
85. Nitsche MA, Paulus W. Excitability changes induced in the human motor cortex by weak transcranial direct current stimulation. *J Physiol* 2000;527(Pt 3):633 639.



Supplementary Figure 1 Schematic of cortical neuron polarization by uniform DC electric field stimulation. A constant current is applied between the parallel Ag/AgCl wires (red bar: anode, blue bar: cathode). The induced currents across a homogenous resistivity, creates a uniform voltage gradient between the anode and cathode. The electric field is the first spatial derivative of the voltage gradient (left two columns). Because the field is uniform, the absolute position of a neuron between the anode and cathode does not matter. (1,2) As current passes in, through, and out the neuron, the neuronal membrane is polarized in a compartment specific manner (blue membrane: induced hyperpolarization; red membrane: induced depolarization). (3) The cell membrane biophysics and cell morphology relative to the electric field determine the distribution of the induced polarization. (4) The relative position of the soma in the dendrite tree determine whether it is depolarized or hyperpolarized by a given direction electric field. (5) Certain morphologies may result in the cell not being polarized, even as dendrite compartment are polarized by electric fields.



Supplementary Figure 2 Polar histogram coherence vector: Neuronal morphology predicts somatic polarization sensitivity to subthreshold electric fields. Summary plot of all neurons recorded and traced, with polar histogram coherence vectors as predictors of somatic polarization per electric field for each neuron. Each cell's mean angle and vector length is indicated by its location on the x and y axis, respectively. Polarization length is indicated by the color and size of the circle representing each cell.



Supplementary Figure 3 Cortical neuron morphologic reconstructions in order of electric field-induced action potential threshold.